Propagation Characteristics of Massive MIMO Measurements in a UMa Scenario at 3.5 & 6 GHz with 100 & 200 MHz Bandwidth

Zhe Zheng*, Jianhua Zhang*, Yawei Yu*, Lei Tian*, and Ye Wu†
*Key Laboratory of Universal Wireless Communications, Ministry of Education,
*State Key Lab of Networking and Switching Technology
Beijing University of Posts and Telecommunications, Beijing, 100876, China
†Huawei Technologies Co., Ltd.
Email: {zhezheng, jhzhang}@bupt.edu.cn

***Abstract*—Massive multi-input and multi-output (MIMO), which uses large-scale antenna arrays to improve spatial efficiency, strengthen performance robustness, etc., is one of primary technologies of 5G wireless communication. To gain further insights into the massive MIMO channel, measurements with the virtual antenna array of the same structure (256 antennas at transmitter and 16 antennas at receiver) are performed in an urban macrocell scenario (UMa) at different frequencies (3.5 & 6 GHz) with different bandwidths (100 & 200 MHz). The enormous collected channel impulse responses enable us to present comparative results including the power delay profile, delay spread and extract angular parameters via SAGE algorithm. Furthermore, angle spread values are illustrated as a direct reflection of massive MIMO channel propagation, then we present comparative channel capacity results. Collectively, these results will shed light on the design of massive MIMO system in UMa environments.**

I. Introduction

Massive multi-input and multi-output (MIMO), which evolves from MIMO technology, is one of primary technologies of 5G wireless communication. With the number of antenna elements deployed on base station growing from tens to hundreds, the channels among different antennas tend to be orthogonal based on theoretic analysis [1], thus the safety, energy efficiency, spatial efficiency and the robustness of massive MIMO system are significantly improved [2]–[4].

Compare with large number of study on massive MIMO system are based on theoretical simulation, there are a lot less results of the system performance of the real radio channels, thus field measurements with massive MIMO antenna arrays have been carried out recently. The measurement in reference [5] was conducted by Aalborg University with 64 Tx antennas at 2.6 GHz center frequency with 50 MHz bandwidth found that an increase in the aperture of the antenna would improve the transmission performance. The measurements in reference [6] were launched in University of Stuttgart with planar, horizontal, and vertical antenna geometries at 2.59 GHz, the results implied that the horizontal antenna arrangement performed best, meanwhile vertical performed worst. Lund university of Sweden has done research on massive MIMO with 128 element antennas at the 2.6 GHz with 50 MHz bandwidth, the performance of two kinds of antenna configurations uniform linear array (ULA) and uniform cylindrical array (UCA) were compared, where ULA would provide better spatial separation than the UCA [7]. A stationary measurement which uses the ULA with 128 elements has been conducted in Beijing Jiaotong Unversity at 1.47 and 4.47 GHz in a stadium [8], and propagation characteristics including pathloss, excess delay and coherence bandwidth at 2, 4 and 6 GHz in an indoor scenario are presented as well [9]. A recent study of massive MIMO channels based on the measurement in an outdoor -to-indoor (O2I) scenario at 3.5 GHz also has been reported [10].

The above field measurements enable us to understand massive MIMO channel better, however, comparative propagation behaviors in UMa scenario among different center frequencies and bandwidths still remains unknown. Thus, in this paper, we focus on the propagation characteristics of massive MIMO in UMa scenario and conduct measurements at 3.5 GHz with 100 & 200 MHz bandwidths and 6 GHz with 200 MHz bandwidth. A large-scale antenna array with 256 elements was utilized at the transmitter (Tx) (shown in Fig. 1b, 1c) and a cylindric antenna array with 16 elements at the receiver (Rx) (shown in Fig. 1a), propagation channels at fixed locations are captured. From the optical view, locations are divided into line-of-sight (LoS) and none line-of-sight (NLoS) cases, comparative results including power delay profile (PDP), root-mean-square (RMS) delay spread (DS), RMS angle spread (AS) and channel capacity have been illustrated. A better resolution of PDP and a larger RMS AS are observed in larger bandwidth at higher frequency, which indicates a better scattering and leads to largest channel capacity at 6 GHz with 200 MHz bandwidth.

The rest of the paper is organized as follow: in Section

II, the measurement equipment and the measurement campaign is described. Section III details the data post-processing and the measurement results. In Section IV, the conclusion is drawn.

II. Channel Measurement

A. Equipment of Measurement

To investigate the channel propagation characteristics of massive MIMO system, extensive channel measurements were performed at Beijing University of Posts and Telecommunications (BUPT), China. The antenna arrays are illustrated in Fig. 1, where an omnidirectional antenna array (ODA) with 56 elements in Fig. 1a and uniform planar antenna array (UPA) with 32 elements in Fig.1b are equipped at Rx and Tx, respectively. However, in our measurement, only 16 elements (marked by red box in Fig.1a) of Rx are active, and a virtual Tx with 256 elements (by shifting the UPA horizontally and vertically as green arrows shows in Fig.1c 8 times) are reconstructed, which collect samples of the massive MIMO channel in a dimension of 256×16. To be noted, the channel was recorded by the Elektrobit PropSound Channel Sounder [11] in a time division way, a stationary environment is assumed when we shift the 32 elements UPA 8 times within a short time, which ensures the rationality of this virtual measurement method [12]. Repeated measurements are conducted at different frequencies (3.5 & 6 GHz) with different bandwidths (100 & 200 MHz) by using the same antenna arrays as described above, which will allow us to compare the massive MIMO propagation characteristics among different measurement cases.

B. Measurement Scenario

The measurement campaigns were conducted near the No.2 Teaching Building of Hongfu campus in BUPT, where the nearby buildings are much lower, which forms a typical urban macro (UMa) cell scenario as shown in Fig. 2(a). The base station (the Tx) was located on top of the 7-floor teaching building with a height being 31m, surrounding buildings are much lower than the base station, and the mobile station (the Rx) was placed on a trolley with 1.8 m high to the ground. The red symbol denotes the location of Tx antenna and yellow section denote its 3-dB lobe width. The Rx position of LoS and NLoS is shown in the map with white point. We divide the fixed locations into LoS and NLoS cases from the optical view, thus location 1 and 2 belong to LoS case while location 3 and 4 belong to NLoS case. Fig. 2(b) shows the position of Tx and Rx antenna that view from ground.

III. Data Analysis and The Measurement Result

By combining the 8 groups of 32×16 antennas channel impulse response (CIR) that calculated form raw data on the base of the timing sequence, the CIRs result of the 256×16 antennas array obtained, and the following data analysis are based on the large antenna array CIR.

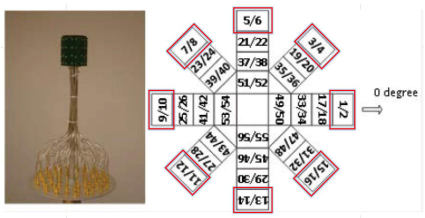

(a) Layout and schematic of ODA in Rx

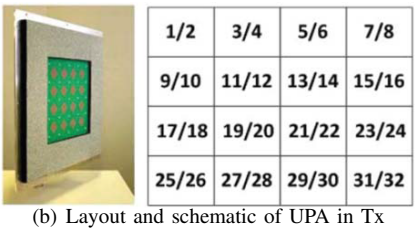

(b) Layout and schematic of UPA in Tx

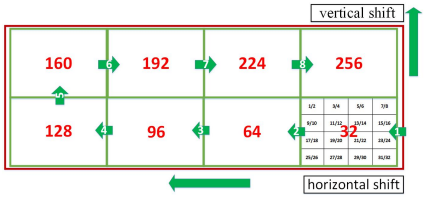

(c) Schematic diagram of 256 elements antenna in Tx

Fig. 1. Layout and schematic of antenna array.

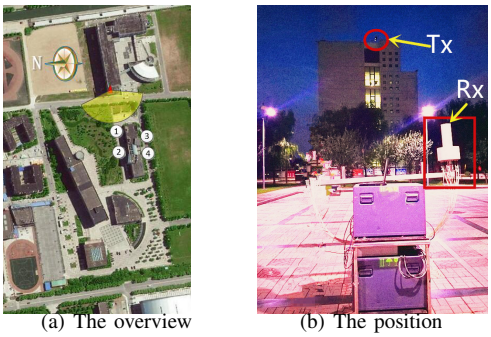

(a) The overview (b) The position

Fig. 2. The overview of the measurement area by Baidu Map, and the setup position of Tx and Rx antenna.

A. PDP

The PDP evaluates the delay dispersions of multiple path components and the power of path l with delay τ_l is calculated as follows:

$$P_l = |h(\tau_l)|^2, l = 1, 2, ..., L \quad (1)$$

where L is the total number of multipaths in the massive MIMO channel. We draw the PDP by listing the average power of 256×16 multipaths and their corresponding excess delays in Fig. 3 and Fig. 4 for LoS and NLoS

cases, respectively. Since the PDP in different locations differ greatly due to the different propagation channels, thus the PDP shown above is for one location in each case.

Fig. 3a shows the comparison result in LoS 1 scenario. As is seen from the picture, 200 MHz have more spikes and burrs than the 100 MHz one in 3.5 GHz. Fig. 3b shows the comparison result of different frequency with same bandwidth, more details of spikes and burrs can be seen in 6 GHz one.

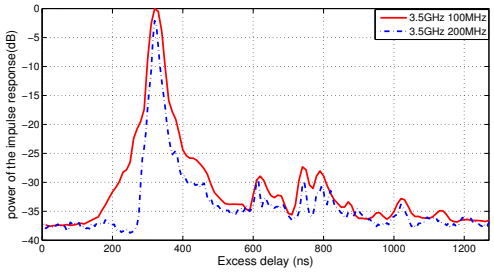

(a) Comparison PDP of 100 & 200 MHz bandwidth in 3.5 GHz

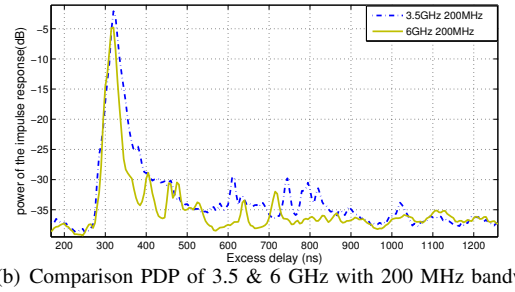

(b) Comparison PDP of 3.5 & 6 GHz with 200 MHz bandwidth

Fig. 3. The comparison of PDP in LoS scenario .

Fig. 4 shows the comparison result in NLoS 1 case, the same as the LoS 1 case, with the increasing of bandwidth and center frequency, more burrs in PDP can be seen. With the richer scattering reflection environment, more path will exist in NLOS scenario.

B. RMS Delay Spread

On the basis of PDP, the statistical characteristics of time dispersion can be calculated. RMS delay spread (DS) τ_{rms} which defined as the square root of the second central moment of PDP can be obtained by

$$\tau_{rms} = \sqrt{\frac{\sum_{r=1}^{L} (\tau_l - \tau_{mean})^2 P_l}{\sum_{r=1}^{L} P_l}} \tag{2}$$

where the mean excess delay τ_{mean} is obtained by

$$\tau_{mean} = \frac{\sum_{l=1}^{L} \tau_l P_l}{\sum_{r=1}^{L} P_l} \tag{3}$$

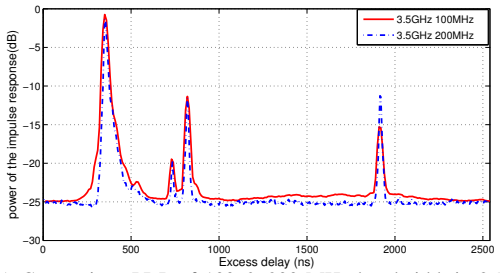

(a) Comparison PDP of 100 & 200 MHz bandwidth in 3.5 GHz

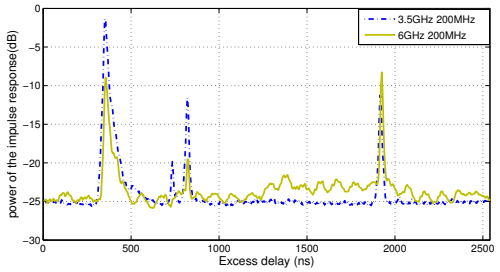

(b) Comparison PDP of 3.5 & 6 GHz with 200 MHz bandwidth

Fig. 4. The comparison of PDP in NLoS scenario .

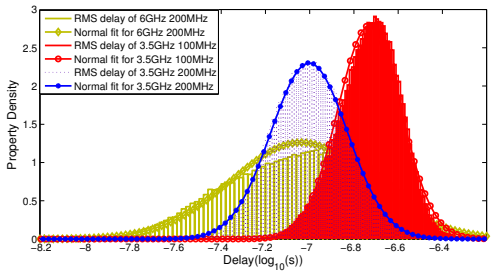

Fig. 5. The RMS delay of LoS scenario.

The noise threshold is set to be 3 dB above the noise floor. The probability density distributions function (PDF) of the RMS DS ($log_{10}(s)$) are the different channel measurements point with the different 1x1 SISO links in each 256x16 measurement at one case, the PDF of LoS and NLoS case are shown in Fig. 5 and Fig. 6 respectively. We use the Gaussian distribution to fit the RMS DS from measurement data. In Fig. 5 of LoS case, the mean value μ of the RMS DS at 3.5 GHz with 100 MHz bandwidth is 186 ns, 3.5 GHz with 200 MHz bandwidth is 100 ns and 6 GHz with 200 MHz bandwidth is 79 ns.

Fig. 6, shows the RMS DS in NLoS case, the delay of 3.5 GHz with 100 MHz bandwidth is 691 ns, 3.5 GHz with 200 MHz bandwidth is 407 ns and 6 GHz with 200 MHz bandwidth is 309 ns. The RMS DS decrease with increasing the bandwidth and frequencyand the results show that the measurement environments have strong impact on the RMS DS, the NLoS case have larger RMS DS due to the richer scattering environment that

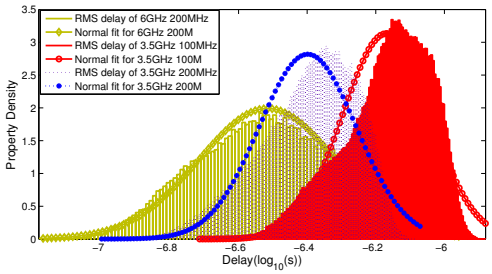

Fig. 6. The RMS delay of NLoS scenario.

TABLE I
MEANS AND STANDARD DEVIATIONS OF RMS DELAY SPREAD

Measurement Case	Delay spread	LOS	NLOS
Frq:3.5 GHz BW:100 MHz	μ log $_{10}(s)$	-6.73	-6.16
	σ log $_{10}(s)$	0.142	0.016
Frq:3.5 GHz BW:200 MHz	μ log $_{10}(s)$	-7.00	-6.39
	σ log $_{10}(s)$	0.173	0.141
Frq:6 GHz BW:200 MHz	μ log $_{10}(s)$	-7.10	-6.51
	σ log $_{10}(s)$	0.132	0.200

generates plentiful longer reflection paths.

Table I illustrates the comparative results of the RMS DS among repeated measurements, which provides insights into the impacts of bandwidth and subcarrier frequencies on propagation parameters. As we can see the tendency of the mean value is getting large with the increase of bandwidth and frequency, the mean value tendency is similar [10] in 3.5 GHz with 100 & 200 MHz bandwidth in outdoor-to-indoor scenario, but the variance does not show a clear tendency.

C. RMS Angle Spread

The multipath channel parameters can be extracted from the CIR by using the well know Spatial Alternating Generalized Expectation maximization (SAGE) algorithm [13]. These channel parameters including ASA, ASD, ESA, ESD are presented in Table II. As we can see from the table, the growth of the mean value of RMS angle spread (AS) is not obvious from 100 to 200 MHz in 3.5 GHz. While comparing the result of 3.5 and 6 GHz, most of the angle expansion are significant, except the ESD. Due to the shorter wavelength, the scattering on the surface of the scatterers become richer, the higher frequencies bring larger AS, but the variance of RMS AS, as well as RMS DS, does not show a clear tendency

D. Channel Capacity

Channel capacity is the key performance indicators of massive MIMO. The capacity of $N \times M$ massive MIMO channel is given by [14], N is the Tx number of antennas, M is the Rx number of antennas.

$$C = \frac{1}{B}\int_B \log_2 \det\left(I_M + \frac{\rho}{N} H\left(f\right) H(f)^H\right) df \quad (4)$$

TABLE II
THE RMS ANGLE SPREAD IN UMA

Scenarios			LoS	NLoS
Frq:3.5 GHz Bw:100 MHz	AoA spread (ASA) log $_{10}(^o)$	μ	1.18	1.58
		σ	0.126	0.117
	AoD spread(ASD) log $_{10}(^o)$	μ	1.28	1.37
		σ	0.048	0.082
	EoA spread(ESA) log $_{10}(^0)$	μ	1.2	1.37
		σ	0.051	0.095
	EoD spread(ESD) log $_{10}(^o)$	μ	1.46	1.48
		σ	0.029	0.051
Frq:3.5 GHz Bw:200 MHz	AoA spread (ASA) log $_{10}(^o)$	μ	1.25	1.64
		σ	0.08	0.086
	AoD spread(ASD) log $_{10}(^o)$	μ	1.21	1.31
		σ	0.059	0.034
	EoA spread(ESA) log $_{10}(^o)$	μ	1.23	1.08
		σ	0.054	0.078
	EoD spread(ESD) log $_{10}(^o)$	μ	1.48	1.46
		σ	0.023	0.014
Frq:6 GHz Bw:200 MHz	AoA spread(ASA) log $_{10}(^o)$	μ	1.66	1.92
		σ	0.057	0.015
	AoD spread(ASD) log $_{10}(^o)$	μ	1.31	1.32
		σ	0.123	0.131
	EoA spread(ESA) log $_{10}(^o)$	μ	1.36	1.42
		σ	0.066	0.05
	EoD spread(ESD) log $_{10}(^o)$	μ	1.31	1.02
		σ	0.186	0.148

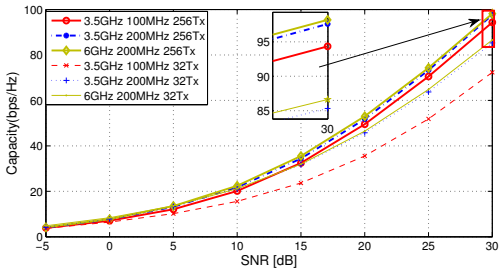

Fig. 7. The capacity comparison of LoS 1 scenario.

where ρ denotes the signal to noise ratio (SNR), $H(f)$ is the channel matrix in frequency domain, B is the bandwidth. The mean channel capacity realized can be given by

$$\widetilde{C}\left(\rho\right) = \frac{1}{K}\sum_{k=1}^{K} \log_2 \det\left(I_M + \frac{\rho}{\beta N} H_r H_r^H\right) \quad (5)$$

where K is the number of channel realizations, H_r is the discrete channel that been realized and β is a common normalization factor for all H_r within one snapshot which satisfies

$$E\left\{\frac{1}{\beta}\left\|H_r\right\|_F^2\right\} = N \cdot M \quad (6)$$

that makes the average channel power gain unitarily [15].

The capacity of MIMO system (32×16) and massive MIMO system (256×16) we get from (5) with different frequency and bandwidth are shown in Fig. 7 & 8. Seen from the detail part of Fig. 7, the capacity increases with the bandwidth and frequency in LoS case, but the

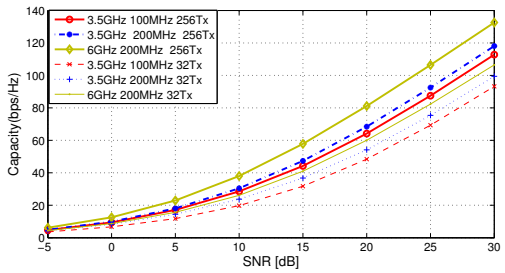

Fig. 8. The capacity comparison of NLoS 1 scenario.

results are close to each other. While in Fig. 8, the NLoS case, obvious capacity gaps among different bandwidths and frequencies are observed, which could be analyzed by the richer scattering in NLoS scenario, thus above the capacity gap would be expanded as compared to the LoS counterpart. Also we can seen from the figure, 3.5 GHz 200 MHz bandwidth has higher capacity than 100 MHz Bandwidth, it probably due to the specific physical layout of the measurement scenario makes the bps/Hz capacity gain more efficient. In addition, we compare the massive MIMO system and the conventional MIMO system, the results show that a better channel performance can be achieved by increasing the antenna number, which provides additional spatial degrees of freedom.

IV. Conclusions

In this paper, we have conducted the virtual massive MIMO (256×16) field measurement in an UMa scenario at two carrier frequencies (3.5 & 6 GHz) with two bandwidths (100 & 200 MHz), aiming to provide insights on the effects of frequency and bandwidth on massive MIMO channel propagation characteristics. The enormous measured samples of CIR enables us to present comparative results of PDP and DS between measurements with different frequencies and bandwidths, which demonstrate a larger DS at lower frequency and narrower bandwidth. Then we extract propagation parameters including azimuth and elevation angles of multipaths via SAGE algorithm and calculate the AS values. Larger AS values at 6 GHz with 200 MHz are observed than the 3.5 GHz with 100 MHz counterpart, which implicates a better scattering at higher frequency and wider bandwidth. Furthermore, we evaluate the above metrics, i.e., DS and AS, on system performance and present comparative capacity results. As expected, measurement at 6 GHz with 200 MHz achieves the highest channel capacity, which can be even 20 bps/Hz higher than that at 3.5 GHz with 100 MHz especially for NLoS locations. Collectively, all the above results based on the virtual massive MIMO field measurement enable us a better understanding of massive MIMO channel propagation.

Acknowledgements

This research is supported in part by National Natural Science Foundation of China (61461136002), and in part by National Science and Technology Major Project of the Ministry of Science and Technology (2015ZX03002008 and 2017ZX03001012-003), and in part by the Ministry of Education - China Mobile Research Fund (MCM20160105). This research is also supported by Huawei Technologies Co., Ltd..

References

[1] F. Rusek, D. Persson, B. K. Lau, E. G. Larsson, T. L. Marzetta, O. Edfors, and F. Tufvesson, "Scaling up MIMO: Opportunities and challenges with very large arrays," *IEEE Signal Processing Magazine*, vol. 30, no. 1, pp. 40–60, 2013.

[2] X. Cheng, B. Yu, L. Yang, J. Zhang, G. Liu, Y. Wu, and L. Wan, "Communicating in the real world: 3d mimo," *IEEE Wireless Communications*, vol. 21, no. 4, pp. 136–144, 2014.

[3] J. Zhang, Y. Zhang, Y. Yu, R. Xu, Q. Zheng, and P. Zhang, "3d mimo: How much does it meet our expectations observed from massive channel measurements?" *IEEE Journal on Selected Areas in Communications*, 2017.

[4] J. Zhang, C. Pan, F. Pei, G. Liu, and X. Cheng, "Three-dimensional fading channel models: A survey of elevation angle research," *IEEE Communications Magazine*, vol. 52, no. 6, pp. 218–226, 2014.

[5] À. O. Martínez, E. De Carvalho, and J. Ø. Nielsen, "Towards very large aperture massive MIMO: A measurement based study," in *Globecom Workshops (GC Wkshps), 2014*. IEEE, 2014, pp. 281–286.

[6] M. Gauger, J. Hoydis, C. Hoek, H. Schlesinger, A. Pascht, and S. ten Brink, "Channel measurements with different antenna array geometries for massive MIMO systems," in *SCC 2015; 10th International ITG Conference on Systems, Communications and Coding; Proceedings of*. VDE, 2015, pp. 1–6.

[7] X. Gao, F. Tufvesson, O. Edfors, and F. Rusek, "Measured propagation characteristics for very-large MIMO at 2.6 GHz," in *Signals, Systems and Computers (ASILOMAR), 2012 Conference Record of the Forty Sixth Asilomar Conference on*. IEEE, 2012, pp. 295–299.

[8] L. Liu, C. Tao, D. W. Matolak, Y. Lu, B. Ai, and H. Chen, "Stationarity investigation of a los massive MIMO channel in stadium scenarios," in *Vehicular Technology Conference (VTC Fall), 2015 IEEE 82nd*. IEEE, 2015, pp. 1–5.

[9] J. Li, B. Ai, R. He, K. Guan, Q. Wang, D. Fei, Z. Zhong, Z. Zhao, D. Miao, and H. Guan, "Measurement-based characterizations of indoor massive MIMO channels at 2 GHz, 4 GHz, and 6 GHz frequency bands," in *Vehicular Technology Conference (VTC Spring), 2016 IEEE 83rd*. IEEE, 2016, pp. 1–5.

[10] C. Xu, J. Zhang, Q. Zheng, and L. Tian, "Measurement-based delay spread analysis of wideband massive MIMO system at 3.5 GHz," in *International Conference on Computational Electromagnetics), 2017 IEEE*. IEEE, 2017, p. in press.

[11] J. Zhang, "Review of wideband MIMO channel measurement and modeling for IMT-Advanced systems," *Chinese Science Bulletin*, vol. 57, no. 19, pp. 2387–2400, 2012.

[12] Y. Hao, J. Zhang, Z. Zheng, and Y. Wu, "The rationality analysis of massive MIMO virtual measurement at 3.5 GHz," in *International Conference on Communications in China(ICCC Workshops)), 2016 IEEE*. IEEE, 2016, p. in press.

[13] B. H. Fleury, M. Tschudin, R. Heddergott, D. Dahlhaus, and K. I. Pedersen, "Channel parameter estimation in mobile radio environments using the SAGE algorithm," *IEEE Journal on selected areas in communications*, vol. 17, no. 3, pp. 434–450, 1999.

[14] A. Paulraj, R. Nabar, and D. Gore, *Introduction to space-time wireless communications*. Cambridge university press, 2003.

[15] D. Tse and P. Viswanath, *Fundamentals of wireless communication*. Cambridge university press, 2005.